Entropy Engineering for Advanced Microwave Ceramics

Supporting Information

Jinquan Zeng[1], Junlei Qi[1, 2*], Kai Wang[3], Bin Wei[3], Minhao Zhang[1], Yiying Chen[1], Jinglei Wang[1], and Yuan-Hua Lin[1*]

[1]State Key Laboratory of New Ceramic Materials, School of Materials Science and Engineering, Tsinghua University, Beijing 100084, China.

[2]State Key Laboratory of New Ceramic Materials, Beijing Tsinghua Institute for Frontier Interdisciplinary Innovation, Beijing 100084, China.

[3]School of Materials Science and Engineering, Henan Polytechnic University, Jiaozuo 454000, China.

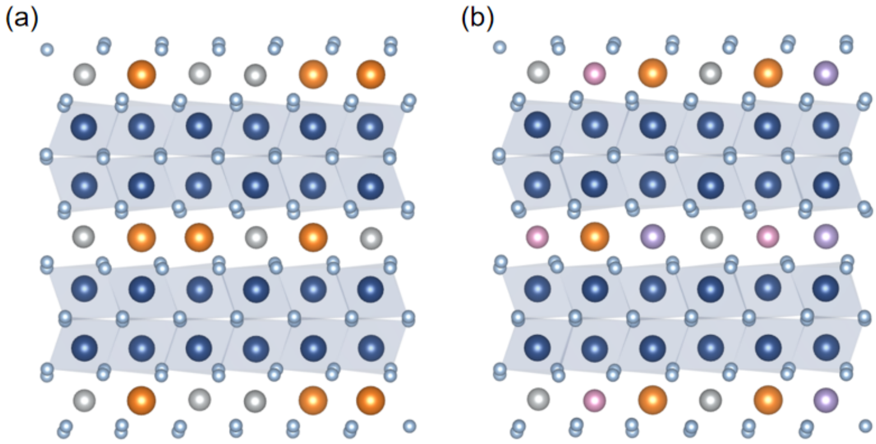

Fig. S1 Super cell structure of (a) (Ni, Mg)$_{0.5}$Nb$_2$O$_6$ and (b) (Ni, Mg, Zn, Co)$_{0.25}$Nb$_2$O$_6$.

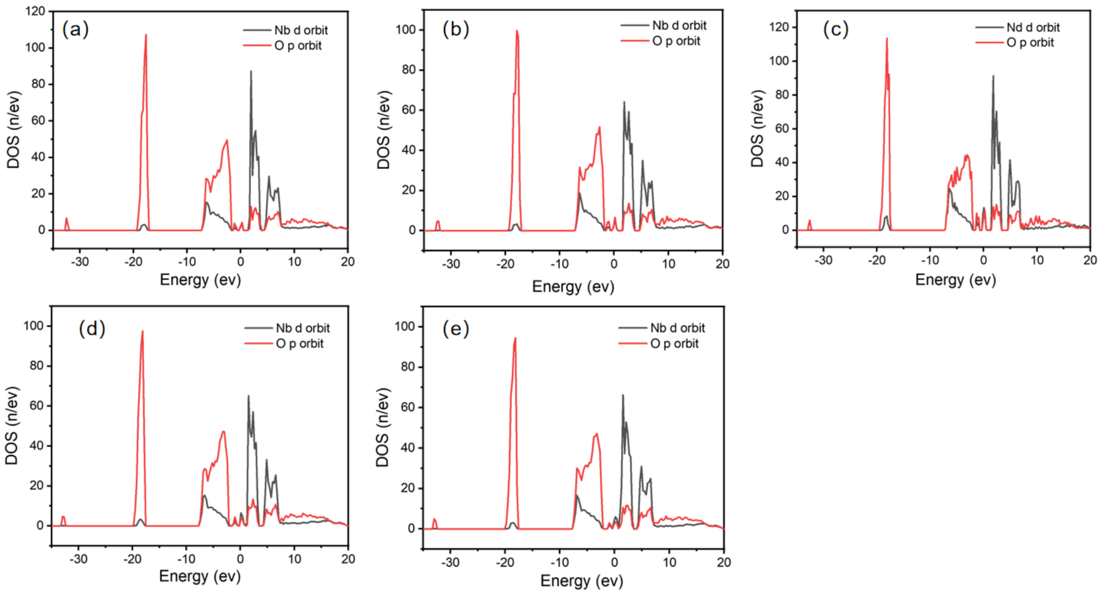

Fig. S2 The partial density of states (PDOS) of (a) $NiNb_2O_6$ (b) $(Ni, Mg)_{0.5}Nb_2O_6$ (c) $(Ni, Mg, Zn)_{1/3}Nb_2O_6$ (d) $(Ni, Mg, Zn, Co)_{0.25}Nb_2O_6$ (e) $(Ni, Mg, Zn, Co, Mn)_{0.2}Nb_2O_6$.

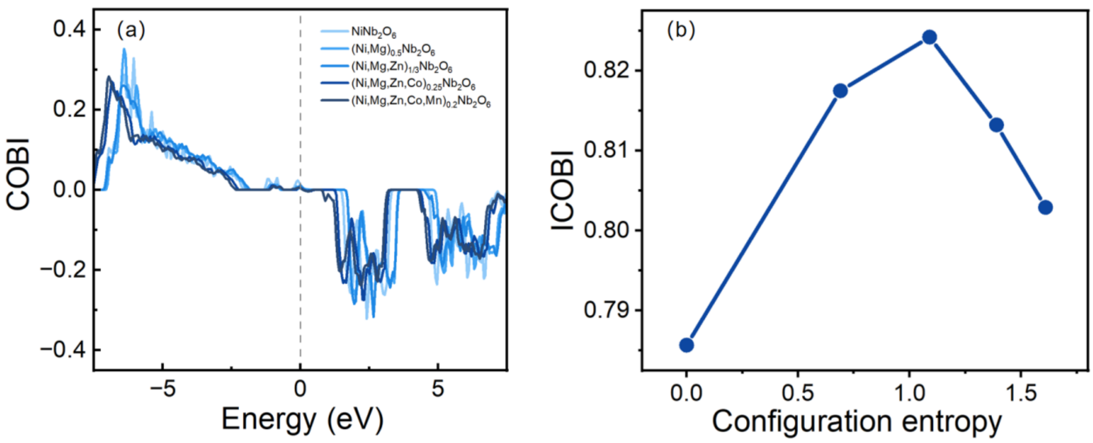

Fig. S3 (a) The calculated crystal orbital bond index (COBI) value from -8 to 8 ev and (b) The integrated crystal orbital bond index (ICOBI) values for Nb–O bonds across low-, medium-, and high-entropy compositions.

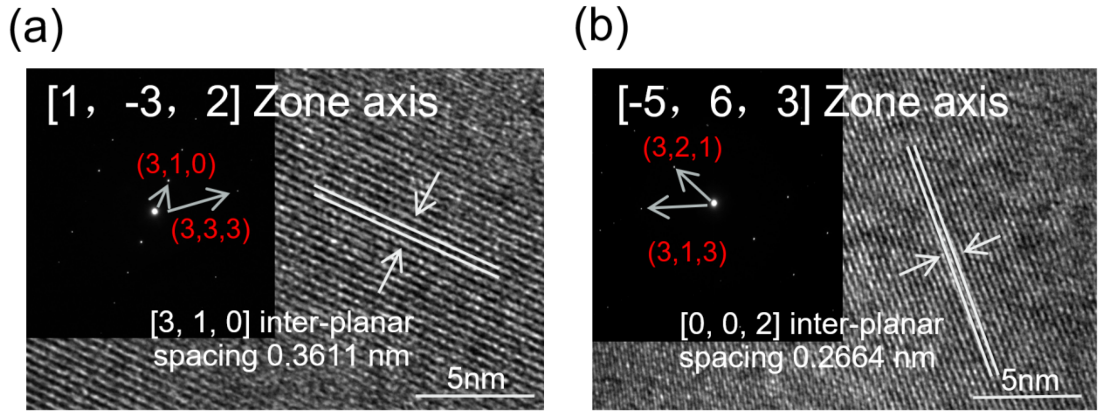

Fig. S4 (a) Medium-entropy samples [1,3,-2] zone axis and (b) high-entropy samples [-5,6,3] zone axis high-resolution transmission electron microscopy (HRTEM).

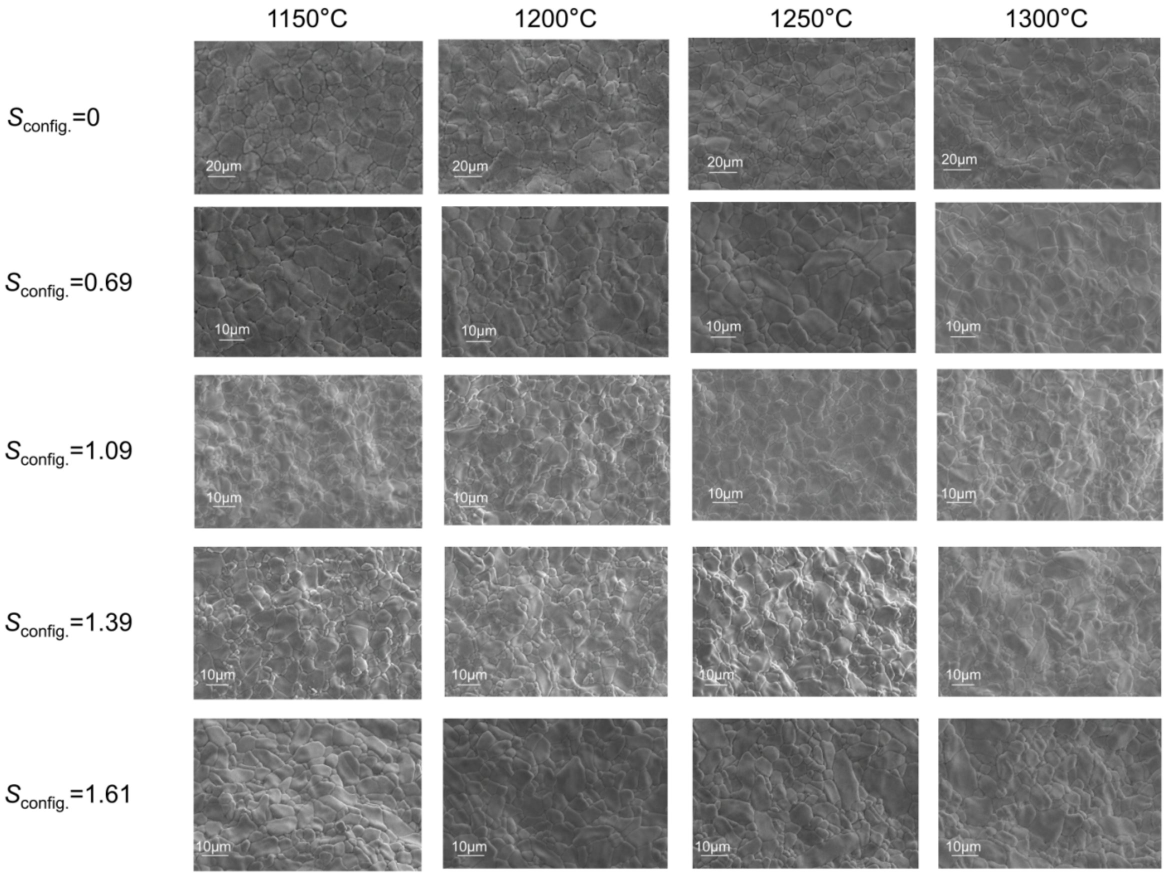

Fig. S5 Scanning electron microscopy (SEM) images of $S_{config.}$ = 0, 0.69, 1.09, 1.39 and 1.61 R from 1150 to 1300°C.

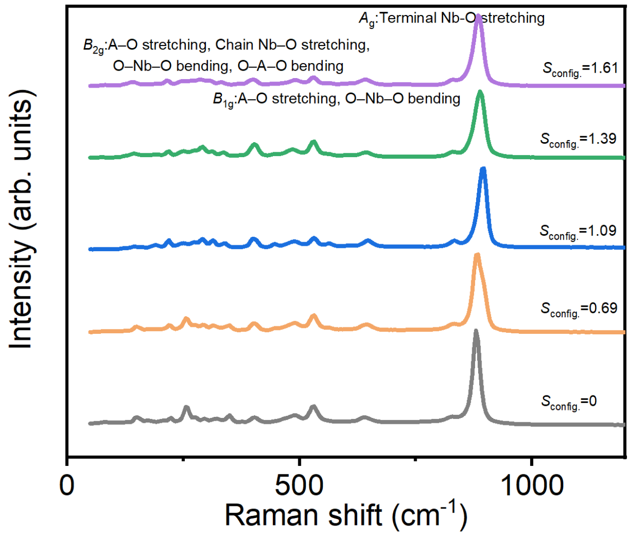

Fig. S6 The room-temperature Raman spectra of samples with different configurational entropy.

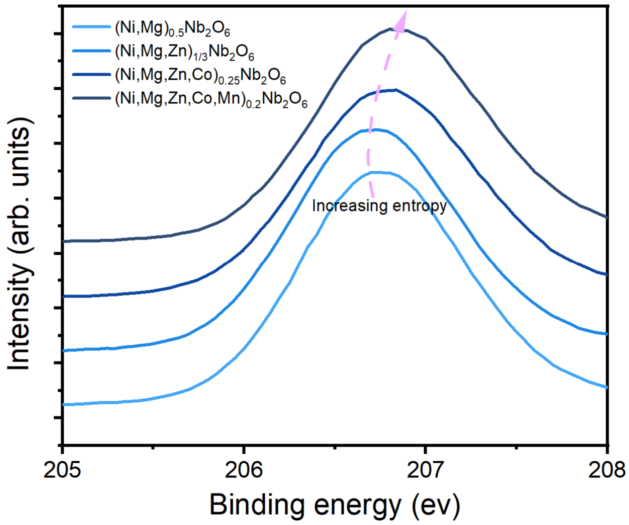

Fig. S7 The Nb 3$d_{5/2}$ peak of X-ray photoelectron spectroscopy (XPS) of samples with different configurational entropy.

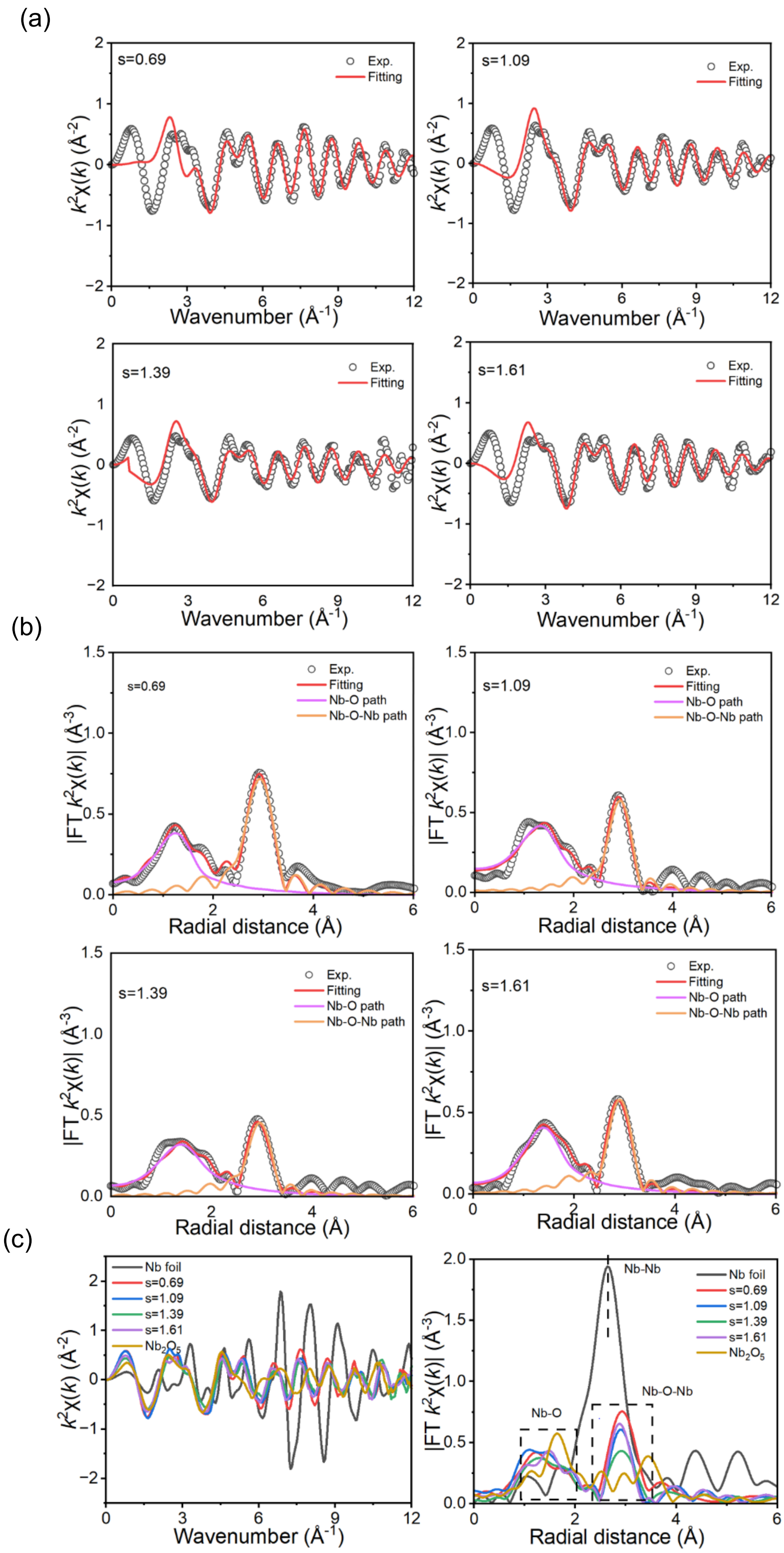

Fig. S8 (a) K space fitting (b) R space fitting (c) summary of *K* and *R* space of ANb_2O_6 with different configurational entropy of X-ray absorption fine structure (EXAFS) analysis.

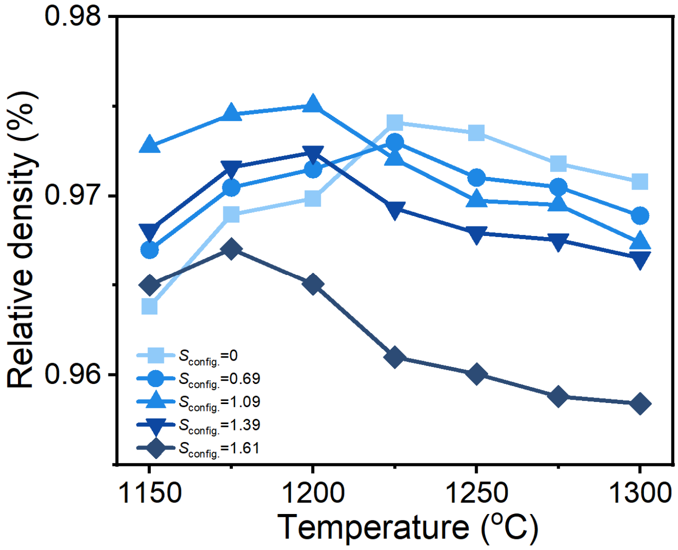

Fig. S9 The relative density of entropy-engineered $NiNb_2O_6$-based ceramics, sintered from 1150 to 1300°C.

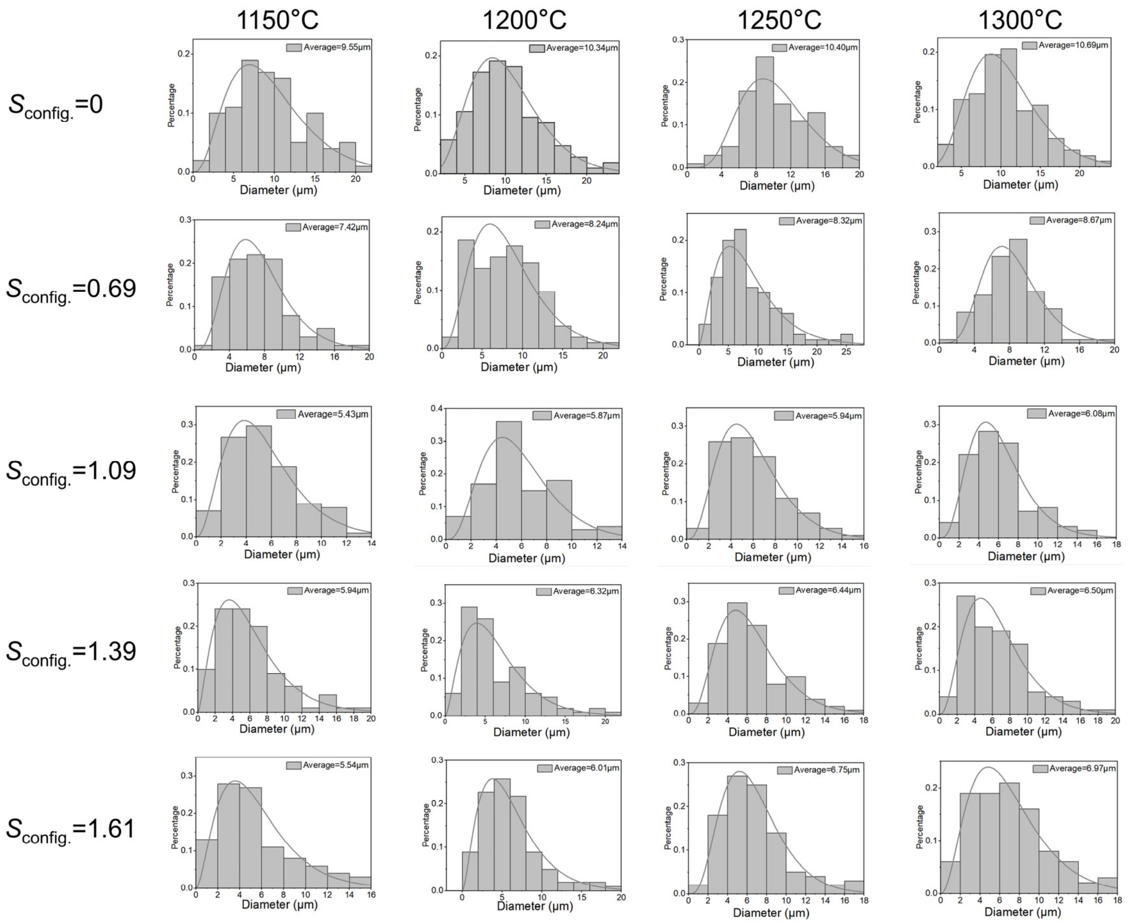

Fig. S10 Grain size distributions of S = 0, 0.69, 1.09, 1.39 and 1.61 R from 1150 to 1300°C.

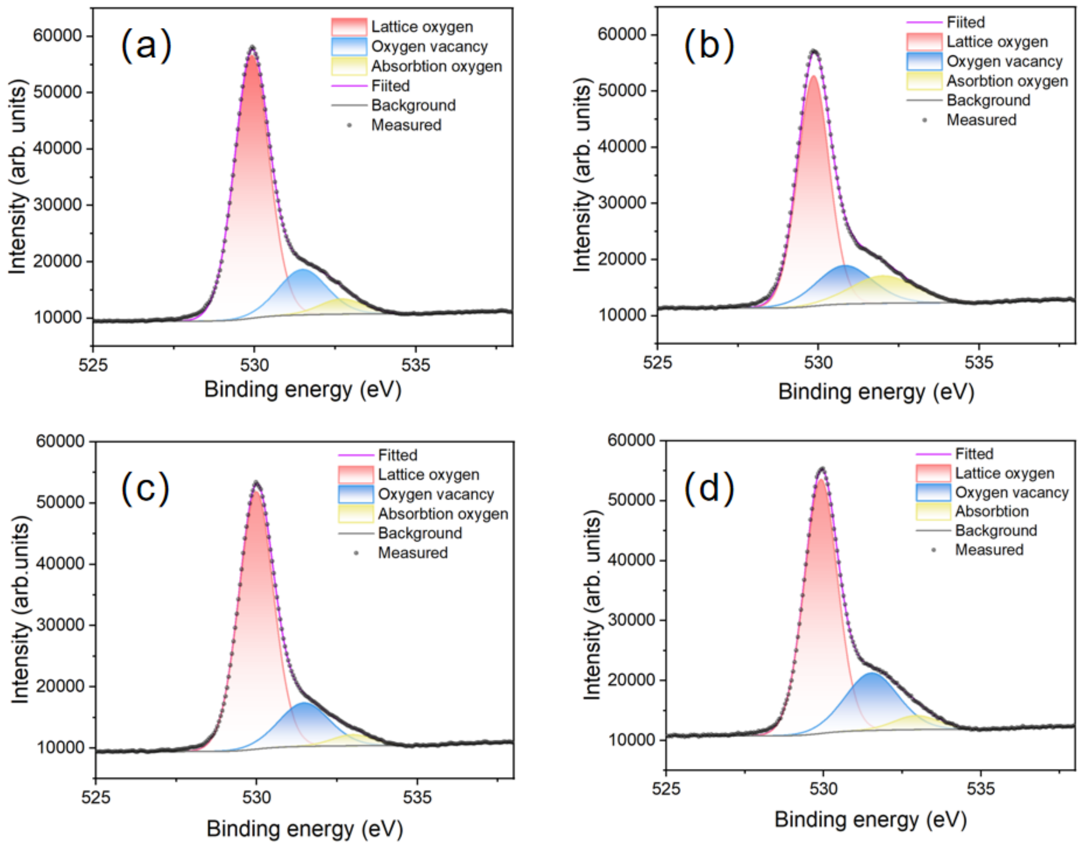

Fig. S11 O 1s XPS spectre of (a) (Ni, Mg)$_{0.5}$Nb$_2$O$_6$ (b) (Ni, Mg, Zn)$_{1/3}$Nb$_2$O$_6$ (c) (Ni, Mg, Zn ,Co)$_{0.25}$Nb$_2$O$_6$ (d) (Ni, Mg, Zn, Co, Mn)$_{0.2}$Nb$_2$O$_6$.

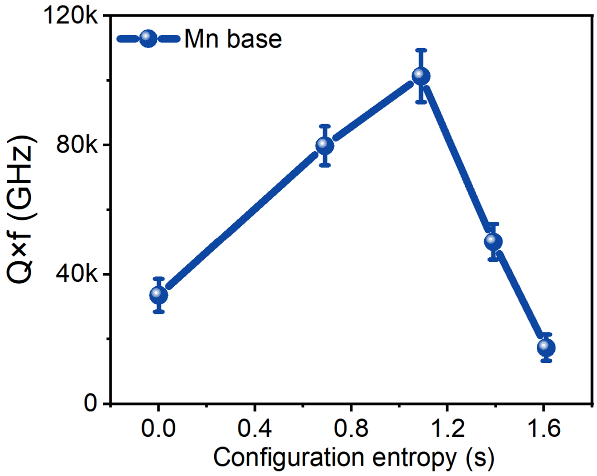

43 **Fig. S12** Q×f with Mn base of $MnNb_2O_6$, $(Mn, Mg)_{0.5}Nb_2O_6$, $(Mn, Mg, Zn)_{1/3}Nb_2O_6$, $(Mn, Mg, Zn,$
44 $Co)_{0.25}Nb_2O_6$, and $(Ni, Mg, Zn, Co, Mn)_{0.2}Nb_2O_6$.

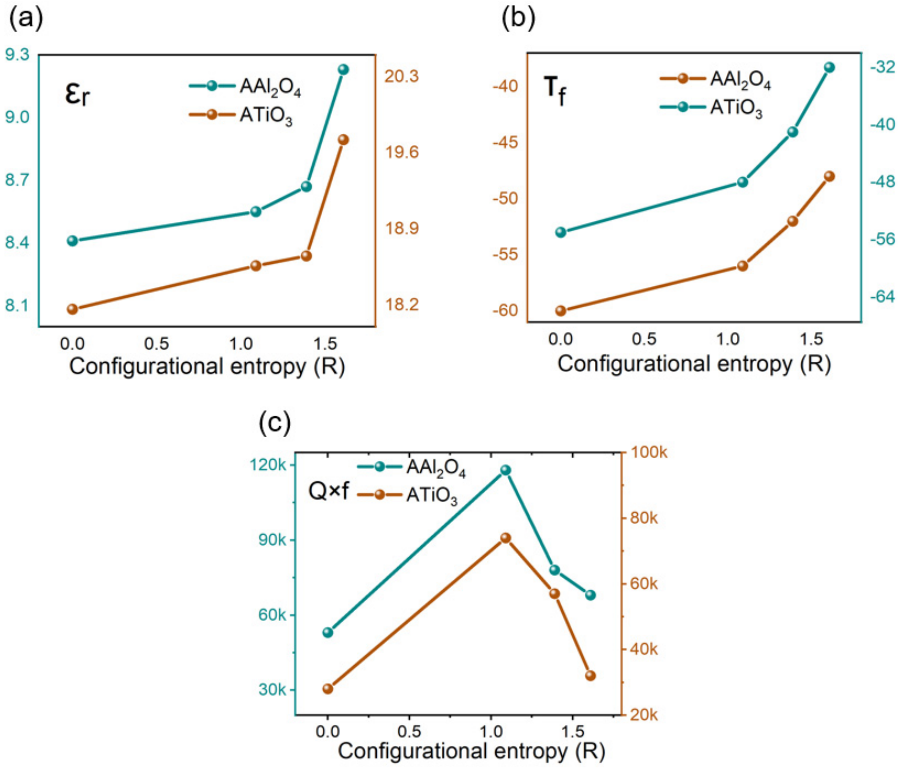

45 **Fig. S13** Microwave dielectric performance of (a) ε_r (b) τ_f (c) Q×f of AAl_2O_4 and $ATiO_3$ systems
46 with different configurational entropy.

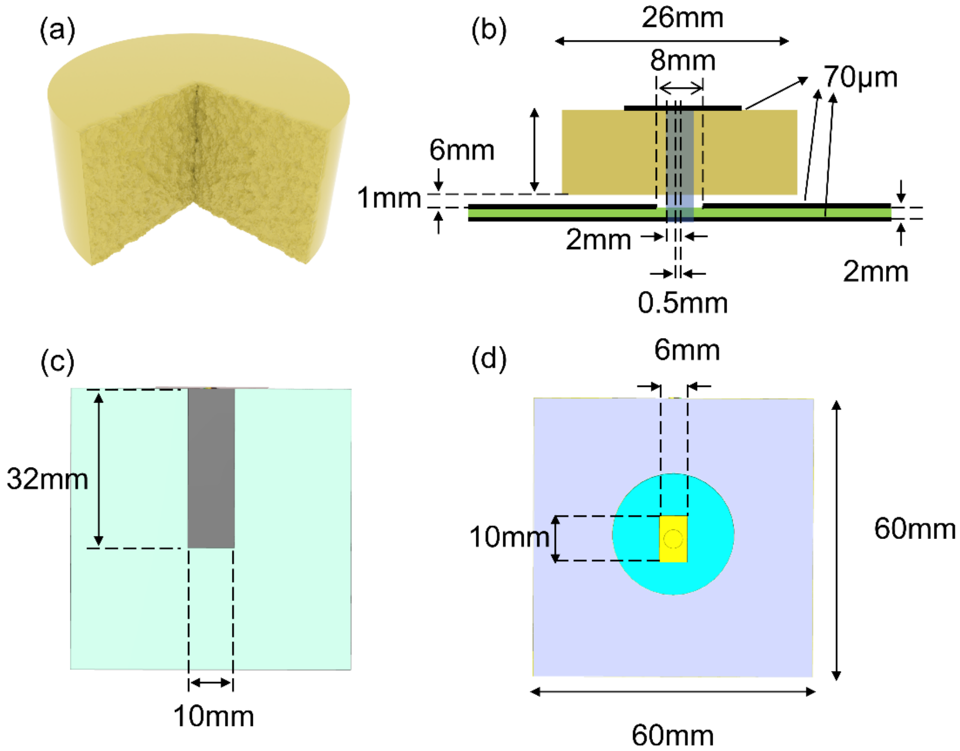

Fig. S14 (a) Schematic of the entropy-engineered ceramic dielectrics. (b–d) Orthographic projections of the fabricated dielectric resonator antenna (DRA): (b) side, (c) bottom, and (d) top views.

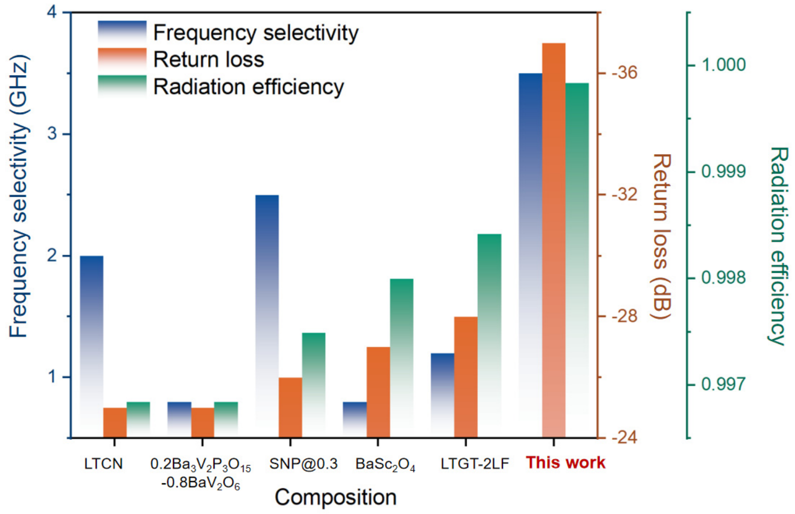

Fig. S15 The comparison of frequency selectivity, return loss and radiation efficiency of recently-reported representative DRAs of microwave dielectrics.

Table. S1 Summary of special quasi-random structure (SQS) supercell specifications for different configurations.

Entropy	A-site composition	SQS supercell specification
Low (S = 0)	Ni	Ordered (all A-sites occupied by Ni)
Low (S = 0.69 R)	$Ni_{0.5}Mg_{0.5}$	12 A-sites: 6 Ni, 6 Mg
Medium (S = 1.09 R)	$Ni_{0.33}Mg_{0.33}Zn_{0.33}$	12 A-sites: 4 Ni, 4 Mg, 4 Zn
Medium (S = 1.39 R)	$Ni_{0.25}Mg_{0.25}Zn_{0.25}Co_{0.25}$	12 A-sites: 3 Ni, 3 Mg, 3 Zn, 3Co
High (S = 1.61 R)	$Ni_{0.2}Mg_{0.2}Zn_{0.2}Co_{0.2}Mn_{0.2}$	12 A-sites: 3 Ni, 3 Mg, 2 Zn, 2 Co, 2 Mn

Table. S2 The element distribution of three grains and the total mapping.

Element/Position	1	2	3	Map Sum
Ni (%)	2.99	5.12	3.88	2.00
Mg (%)	1.76	1.49	1.34	2.14
Zn (%)	1.09	0.89	0.97	0.96
Co (%)	2.80	3.70	2.91	2.37
Mn (%)	1.98	1.73	1.62	2.16
Nb (%)	29.56	31.15	32.05	27.48
O (%)	59.81	55.92	57.23	62.90

Table. S3 Summary of EXAFS fitting parameters for the Nb K-edge

s	Path	R (Å)	σ^2 (Å^2)	CN	ΔE_0 (eV)	R factor
			Nb K edge (S_0^2=0.97)			
0.69	Nb–O	1.87±0.01	0.205	5.17±0.69	-13.5	0.0190
1.09	Nb–O	1.95±0.02	0.247	6.08±0.43	-1.9	0.0049
1.39	Nb–O	1.97±0.01	0.262	5.39±0.51	1.6	0.0199
1.61	Nb–O	1.99±0.01	0.310	4.86±0.18	-0.4	0.0025

Table. S4 Statistical results of Pearson correlation analysis between configurational entropy and microwave dielectric properties

Pearson correlation	ε_r	Q×f	τ_f
r	0.85	No significant linear correlation	0.94

Pearson correlation analysis reveals that ε_r and τ_f are positively correlated with $S_{config.}$, while Q×f displays a non-monotonic trend, reaching a maximum at intermediate configurational entropy compositions. The dataset contains n=5 samples, corresponding to compositions with $S_{config.}$ values of 0, 0.69, 1.09, 1.39, and 1.61 of $ANbO_6$, respectively. Given the limited number of compositional variants examined in this study, the statistical outcomes reported herein are valid solely for the measured experimental samples.

We assessed the correlation between $S_{config.}$ and microwave dielectric performance using Pearson correlation (r): $r = \dfrac{\sum_{i=1}^{n}(x_i - \bar{x})(y_i - \bar{y})}{\sqrt{\sum_{i=1}^{n}(x_i - \bar{x})^2 \cdot \sum_{i=1}^{n}(y_i - \bar{y})^2}}$

Table. S5 The optimized sintering temperature

Composition	Optimized sintering temperature (°C)
$NiNb_2O_6$	1225
$Ni_{0.5}Mg_{0.5}Nb_2O_6$	1225
$Ni_{0.33}Mg_{0.33}Zn_{0.33}Nb_2O_6$	1200
$Ni_{0.25}Mg_{0.25}Zn_{0.25}Co_{0.25}Nb_2O_6$	1200
$Ni_{0.2}Mg_{0.2}Zn_{0.2}Co_{0.2}Mn_{0.2}Nb_2O_6$	1175

Table. S6 The performance comparison between the DRA constructed from medium-entropy ANb_2O_6 and the reported DRAs.

Resonant frequency (GHz)	Selective width >-5db (GHz)	Return loss (db)	Conversion efficiency (%)	Ref.
2.6	2.0 (1.5-3.5)	-25 (0.316%)	99.684%	[1]
11.1	2.5 (10-12.5)	-26 (0.251%)	99.749%	[2]
6.0	1.2 (5.2-6.4)	-28 (0.158%)	99.842%	[3]
8.1	0.8 (7.5-8.3)	-25 (0.316%)	99.684%	[4]
5.8	0.8 (5.4-6.2)	-27 (0.200%)	99.800%	[5]
6.8	3.5 (5.0-8.5)	-37 (0.016%)	99.984%	This work

Reference:

1 Guo, H.-H. *et al.* Design of a high-efficiency and -gain antenna using novel low-loss, temperature-stable $Li_2Ti_{1-x}(Cu_{1/3}Nb_{2/3})_xO_3$ microwave dielectric ceramics. *ACS Appl. Mater. Interfaces* **13**, 912–923 (2021). https://doi.org/10.1021/acsami.0c18836

2 Wu, F. *et al.* P^{5+}- Enhanced novel samarium niobate ultralow-loss microwave ceramics as dielectric resonator for x-band antenna applications. *Adv. Funct. Mater.* **35**, 2421225 (2025). https://doi.org/10.1002/adfm.202421225

3 Wang, Z., Guo, H., Huang, Y. & Li, Y. Synergistic dual-phase and microstructure engineering toward temperature-stable, ultra-low loss Li_2TiO_3-based microwave dielectric ceramic. *Adv. Funct. Mater.* **36**, e18002 (2025). https://doi.org/10.1002/adfm.202518002

4 Wang, C. H. *et al.* Novel temperature-stable (1-x)$Ba_3V_2P_3O_{15}$-xBaV_2O_6 composite ceramics with ultralow sintering temperature and low dielectric loss for dielectric resonator antenna applications. *Adv. Funct. Mater.* **36**, e22167 (2025). https://doi.org/10.1002/adfm.202522167

5 He, G. *et al.* $BaSc_2O_4$: A novel AB_2O_4-type low-k microwave dielectric ceramic with giant positive τ_f for 5g/6g frequency compensation. *Adv. Funct. Mater.* **36**, e28138 (2025). https://doi.org/https://doi.org/10.1002/adfm.202528138